Journal of Sound and Vibration (2002) **258**(2), 309–325
doi:10.1006/jsvi.5178, available online at http://www.idealibrary.com on IDEAL®

VIRTUAL REALITY OF SOUND GENERATED FROM VIBRATING STRUCTURES

S. J. Kim and J. Y. Song

Department of Aerospace Engineering, College of Engineering, Seoul National University, Shinrim-Dong Kwanaku, Seoul 151-742, *South Korea. E-mail: sjkim@snu.ac.kr*

(*Received* 10 *July* 2001, *and in final form* 7 *March* 2002)

The advancement of virtual reality (VR) technology in cyberspace is amazing, but its development is mainly concentrated on the visual part. In this paper, the development of VR technology to produce sound based on the exact physics is studied. Our main concern is on the sound generated from vibrating structures. This may be useful, for example, in apprehending sound field characteristics of an aircraft cabin in design stage.

To calculate sound pressure from curved surface of a structure, a new integration scheme is developed in boundary element method. Several example problems are solved to confirm our integration scheme. The pressure distributions on a uniformly driven sphere and cylinders are computed and compared with analytic solutions, and radiation efficiency of a vibrating plate under one-dimensional flow is also calculated. Also, to realize sound through computer simulation, two concepts, "structure-oriented analysis" and "human-oriented analysis", are proposed. Using these concepts, virtual sound field of an aircraft cabin is created.

1. INTRODUCTION

The theory of acoustics was established in the 19th century by Stokes and Rayleigh. Many analytic and numerical approaches of calculating sound pressure are concentrated on calculating sound pressure generated from vibrating plates [1, 2]. For curved structures, radiating sound field of a cylindrical structure was analyzed [3] and a thin sphere was used in the analysis of sound field with consideration of interaction between structure and exterior sound field [4]. A structure, which is composed of a cylindrical plate and shell, was used in the analytic analysis of noise of an aircraft cabin [5].

The concept of virtual experiment can be defined as follows. "The virtual experiment is an enhanced numerical simulation which serves not only resulting data but also feeling of resulting environments to human beings." A conceptual picture of a virtual noise experiment is shown in Figure 1. In Figure 1, a person can hear noise induced by vibration of an airplane, not in real space but through a headphone which is connected to a computer on which real physics are projected. To project a continuous real sound field to a digitized cyberspace, we introduce two concepts, "structure-oriented analysis" and "human-oriented analysis".

In this study, sound pressure is calculated using boundary element method (BEM). Linear 3-node triangular and 4-node rectangular elements are used, and a new integration technique is developed for integration on curved surfaces. Also, a technique of considering interactions among structure, interior and exterior sound field is developed. To consider

0022-460X/02/$35.00

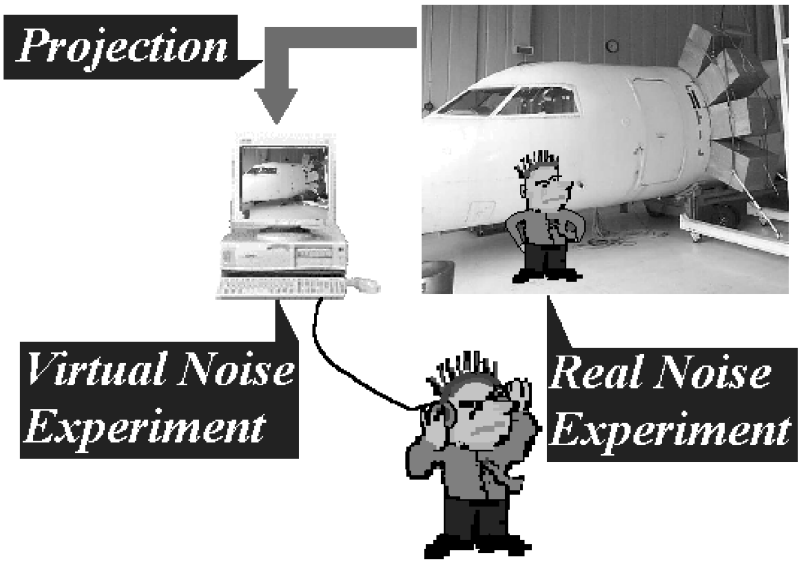

Figure 1. Concept of the virtual noise experiment.

impedance characteristics of a structure, eigenvalues and mode shapes of finite element method (FEM) [6] model of structure are used.

For the verification of our integration scheme, sound pressure distributions on uniformly driven sphere and cylinders are computed, and the radiation efficiencies of a vibrating plate under one-dimensional flow are also calculated. Then, virtual realization of a sound field from a vibrating aircraft cabin is chosen to show the applicability of the developed virtual reality (VR) technology.

2. GOVERNING EQUATIONS OF SOUND FIELD

When there is one-dimensional flow along x-axis, the following potential function and boundary condition can be introduced to obtain sound pressure [7].

$$\left[\nabla^2 - \frac{1}{c^2}\left(-\mathrm{j}\omega + V\frac{\partial}{\partial x}\right)^2\right]\hat{\psi}(x, y, z, \omega) = 0. \tag{1}$$

The boundary condition is as follows:

$$\frac{\partial\hat{\psi}}{\partial n} = \left(-\mathrm{j}\omega + V\frac{\partial}{\partial x}\right)\hat{u}_n(x_s, y_s, z_s, \omega). \tag{2}$$

Using the Green function G, $\hat{\Psi}$ can be derived as

$$\hat{\psi}(x, y, z, \omega) = \int_S \left[\hat{\Psi}\frac{\partial G}{\partial n} + G(x, y, z|x_s, y_s, z_s)\left(-\mathrm{j}\omega + V\frac{\partial}{\partial x}\right)\hat{u}_n\right] \mathrm{d}S. \tag{3}$$

Here, the Green function G is defined as

$$G(x, y, z|x_s, y_s, z_s) = -\frac{\exp(\mathrm{j}k[M(x - x_s) + R]/1 - M^2)}{2\pi R\sqrt{1 - M^2}}, \tag{4}$$

where

$$R = \sqrt{(x - x_s)^2 + (1 - M^2)[(y - y_s)^2 + (z - z_s)^2]}. \tag{5}$$

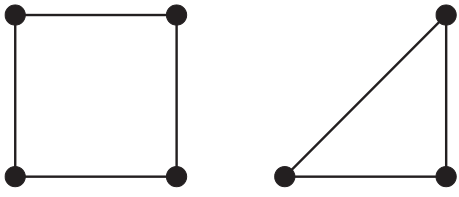

Figure 2. Two linear BEM elements used in this study.

Then, sound pressure at position (x, y, z) can be obtained:

$$\begin{aligned}\hat{p}(x,y,z,\omega) &= -\rho\left(-\mathrm{j}\omega + V\frac{\partial}{\partial x}\right)\hat{\Psi}(x,y,z,\omega)\\ &= -\rho\left(-\mathrm{j}\omega + V\frac{\partial}{\partial x}\right)\left[\int_S\left[\hat{\Psi}\frac{\partial G}{\partial n} + G(x,y,z|x_s,y_s,z_s)\left(-\mathrm{i}\omega\hat{u}_n + V\frac{\partial \hat{u}_n}{\partial x}\right)\right]\mathrm{d}S\right]\\ &= \left[\int_S\left[-\rho\left(-\mathrm{j}\omega + V\frac{\partial}{\partial x}\right)\hat{\Psi}\right]\frac{\partial G}{\partial n}\mathrm{d}S\right]\left(\rightarrow \int_S \hat{p}\frac{\partial G}{\partial n}\mathrm{d}S\right)\\ &\quad + \rho\omega^2\int_S G\hat{u}_n\,\mathrm{d}S + \mathrm{j}\rho\omega V\int_S G\frac{\partial \hat{u}_n}{\partial x}\mathrm{d}S + \mathrm{j}\rho\omega V\int_S\frac{\partial G}{\partial x}\omega\,\mathrm{d}S - \rho V^2\int_S\frac{\partial G}{\partial x}\frac{\partial \omega}{\partial x}\mathrm{d}S.\end{aligned} \tag{6}$$

Using BEM, we can convert equation (6) into a matrix form.

After integrating equation (6) moving observer's position (x, y, z) all over the nodes on the surface, the following matrix form, which is the relationship between sound pressures on the surface and displacements of the surface in the surface normal direction, can be made:

$$[B]\{P\} = [C]\{U_n\}. \tag{7}$$

In the case of 4-node square elements, diagonal terms of matrices become singular. Those singular terms are integrated after dividing the square element into two triangles [6, 7].

Using equation (8), equation (7) can be rewritten to equation (9), which is our final form

$$\frac{\partial\{P\}}{\partial n} = -\rho\frac{\partial\{V_n\}}{\partial t} = -\rho j\omega\{V_n\} = \rho\omega^2\{U_n\}, \tag{8}$$

$$[B]\{P\} = [D]\{V_n\}. \tag{9}$$

The elements used in this study are shown in Figure 2.

3. HOW TO OBTAIN THE IMPEDANCE MATRIX OF STRUCTURES

To consider interactions between structure and sound field, the inverse of structural impedance matrix is needed. In this study, this matrix is obtained by using eigensolutions of structure as

$$Z_{ik}^{-1}(\omega) = \mathrm{j}\omega\alpha_{ik}(\omega) = \mathrm{j}\omega\sum_{r=1}^{N}\frac{{}_r\phi_i\,{}_r\phi_k}{m_r(\omega_r^2 - \omega^2 + \mathrm{j}\eta_r\omega_r^2)}. \tag{10}$$

When ω is close to ω_r in equation (10), α_{il} can be rewritten approximately as follows:

$$\alpha_{il}(\omega) \approx \sum_{r=1}^{n(\leqslant N)} \frac{{}_r\phi_i r\phi_l}{m_r(\omega_r^2 - \omega^2 + \mathrm{j}\eta_r\omega_r^2)}. \tag{11}$$

Here, n is an integer which is not greater than N. If $\omega_r (r = 1, 2, \cdots, N)$ are located remotely enough, n can be assumed as 1.

This approach has the following merits over the ordinary approach [8, 9]:

1. It removes the process of getting the inverse matrix of $[Z]$. So, numerical errors resulted from the inverse process can be removed.
2. Erroneous effects resulted from inaccuracy of FEM model in high-frequency region will be removed because eigenvalues and mode shapes of only the selected frequency range are used.
3. Some useful information on characteristics of radiating sound can be observed by looking at the mode shapes.

MSC NASTRAN [10] is used in calculating the eigensolution of a structure.

4. ANALYSIS OF SOUND FIELD

Governing equations of interior and exterior sound field can be rewritten, respectively, from equation (9) in the following form:

$$[B]_i\{P\}_i = [D]_i\{V_n\}_i, \tag{12}$$

$$[B]_e\{P\}_e = [D]_e\{V_n\}_e. \tag{13}$$

Consider the continuity of displacements on the surface of structure,

$$\{v_n\} = \{V_n\}_i = \{V_n\}_e. \tag{14}$$

Then, by the equilibrium of forces on the surface of structure,

$$[Z]\{v_n\} = \{F\} - \{F\}_{fluid} = \{F\} - [\{F\}_{fluid_i} + \{F\}_{fluid_e}]. \tag{15}$$

From equations (12), (14) and (15), a equilibrium equation on the surface with respect to the interior sound field and the structure can be derived:

$$\Big[[B]_i + [D]_i[T][Z]^{-1}[T]^{\mathrm{T}}[A_d]\Big]\{P\}_i + [D]_i[T][Z]^{-1}[T]^{\mathrm{T}}[A_d]\{P\}_e = [D]_i[T][Z]^{-1}\{F\}. \tag{16}$$

Equation (16) can be rewritten as follows:

$$[P_{11}]\{P\}_i + [P_{12}]\{P\}_e = [Q_1]\{F\}, \tag{17}$$

where

$$[P_{11}] \equiv [B]_i + [D]_i[T][Z]^{-1}[T]^{T}[A_d], \tag{18}$$

$$[P_{12}] \equiv [D]_i[T][Z]^{-1}[T]^{\mathrm{T}}[A_d], \tag{19}$$

$$[Q_1] = [D]_i[T][Z]^{-1}. \tag{20}$$

Then, we can derive an equilibrium equation on the surface with respect to the exterior sound field and the structure using equations (13)–(15):

$$[P_{21}]\{P\}_i + [P_{22}]\{P\}_e = [Q_2]\{F\}, \tag{21}$$

where

$$[P_{21}] \equiv [D]_e[T][Z]^{-1}[T]^{\mathrm{T}}[A_d], \tag{22}$$

$$[P_{22}] \equiv [B]_e + [D]_e[T][Z]^{-1}[T]^{\mathrm{T}}[A_d], \tag{23}$$

$$[Q_2] = [D]_e[T][Z]^{-1}. \tag{24}$$

From equation (17) and (21), we can derive a matrix equation as follows:

$$\begin{bmatrix} [P_{11}] & [P_{12}] \\ [P_{21}] & [P_{22}] \end{bmatrix} \begin{Bmatrix} \{P\}_i \\ \{P\}_e \end{Bmatrix} = \begin{Bmatrix} [Q_1]\{F\} \\ [Q_2]\{F\} \end{Bmatrix}. \tag{25}$$

5. HOW TO MAKE VIRTUAL SOUND

The convergence of virtual sound is different from the conventional convergence concept in mathematics. ''Virtual sound converges to real sound'' means virtual sound and real sound give same feelings to the hearer. So, to efficiently obtain converged virtual sound, two dominant factors of sound should be considered, which are characteristics of structural vibration and human's hearing.

To consider the structural characteristics, structure-oriented analysis concept is devised; to consider human's characteristics, human-oriented analysis concept is devised; and to consider both concepts, sound pressure in frequency domain should be obtained before calculating sound pressure in time domain.

When sound pressures on surface in frequency domain are obtained by equation (25), sound pressures at an observer's position in a sound field can be calculated using the matrix form of equation (6). Using these solutions, sound pressure function of time is given by equation (26).

$$p(t) = \sum_{i=0}^{\infty} \hat{\boldsymbol{P}}_i \exp(\mathrm{j}\omega_i t) \approx \sum_{i=0}^{N-1} \hat{\boldsymbol{P}}(i) \exp(\mathrm{j}\omega(i)t). \tag{26}$$

In equation (26), the determination of N and $\omega(i)$ is very important for the convergence of virtual sound. For this, structure-oriented analysis and human-oriented analysis are introduced.

Structure-oriented analysis is the concept that $\omega(i)$ is selected among structure's natural frequencies and is developed for the following three reasons:

1. $\omega(i)$, at which radiating sound pressure from structure is relatively high, is among the natural the frequencies of structure.
2. The frequency response function of structure can be more easily calculated by using equation (11) instead of equation (10).
3. The effects of erroneous terms of FEM model in high frequencies can be removed by structure-oriented analysis, because the structural properties of only the selected natural frequencies will be used in calculations.

However, calculation of sound pressure at all eigenmodes takes too much time, and mode shapes of closely packed eigenmodes are so alike that their radiation characteristics are almost indistinguishable by human ear. Therefore, it is somewhat redundant to calculate sound pressure at all natural frequencies. To treat such problems, human-oriented analysis is introduced. The concept of human-oriented analysis is devised to divide the frequency domain using the ratio of the octave. Basically, frequency domain is

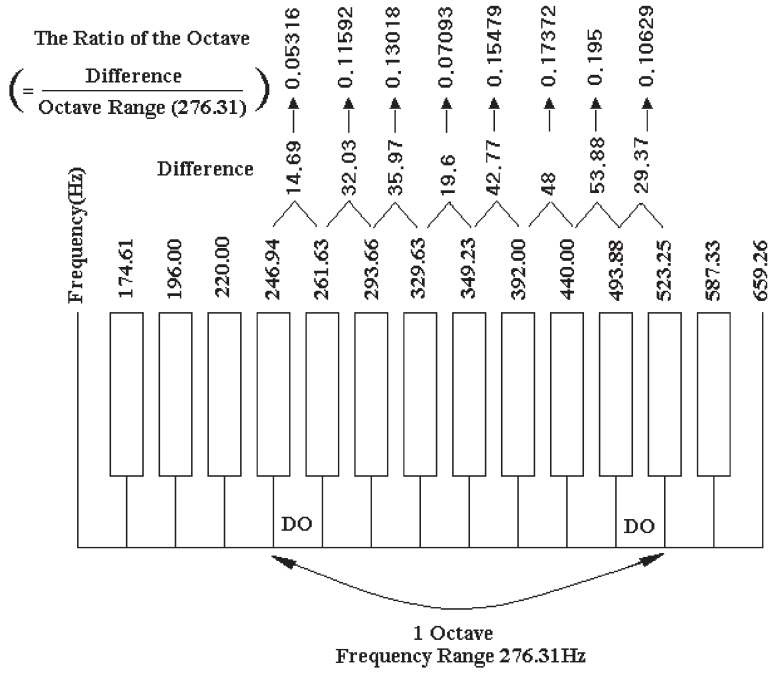

Figure 3. The ratio of the octave.

divided using an octave scale, and if necessary, the musical interval will be divided again by the ratio of the octave. The ratio of the octave is illustrated in Figure 3. This concept is similar to the schemes of virtual realization in computer graphics which express things using polygons.

Therefore, the frequency selecting scheme used in this study can be summarized as follows:

1. Compute eigensolutions of structure.
2. Determine a frequency region where the values of eigenvalues and mode shapes can be calculated accurately judging from d.o.f. of FEM model and spectral densities of external forces.
3. Divide the frequency region selected in step 2 using the concept of human-oriented analysis.
4. Select frequencies among the natural frequencies which are the closest to the frequencies determined in step 3.

After selecting the frequencies, sound pressure is calculated at each frequency. Using these frequencies and pressures, we compute an approximate pressure function which is given in equation (26). Then, data at each time step can be prepared by an approximate pressure function. The final results are obtained in the form of a wave file. While wave files have several kinds of formats [11], we adopted 16-bit, stereo format with 44 kHz of sampling ratio.

6. INTEGRATION ON CURVED SURFACES

To integrate a BEM element on a curved surface, local co-ordinate systems defined at each integration point are created and the co-ordinate system on each element is

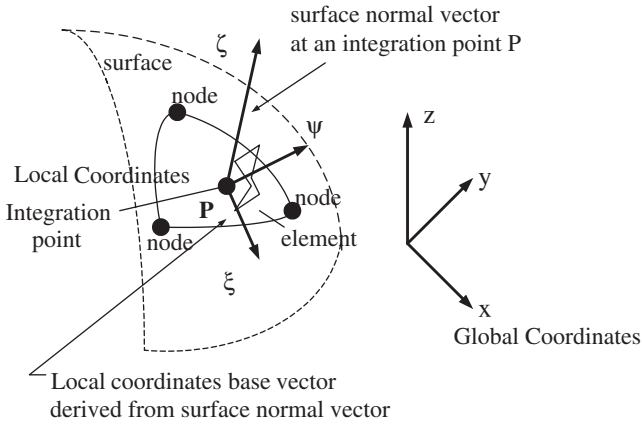

Figure 4. Relationship between an integration point and local co-ordinate system.

transferred from global to a corresponding local co-ordinate system. The local co-ordinate system at an integration point is obtained using normal vectors of the surface at the integration point, and the process of obtaining the local co-ordinate system is as follows:

1. Calculate normal vectors of a surface at each integration point using analytic solutions. The accuracy of normal vector is a very important factor, so it should be obtained using the exact geometry data (or CAD data), not the FEM mesh data.
2. Using the normal vector, derive two orthonormal base vectors of the given element.
3. Then, the two orthonormal base vectors are the base vector of 2-D local space in which integration at a given integration point is performed.

As for normal vectors, at first, one local co-ordinate system is used on each element. In other words, on an element, the local co-ordinate system is fixed, regardless of the position of the integration point. In this case, the normal vectors at the element's center point are obtained by the arithmetic average of normal vectors at each node in the element (however, it produces poor result as shown in Figure 6).

Everstine and Henderson [4] use first order numerical integration and obtain good results. From this, we realize that normal directions at integration points are very important, and we use a different local co-ordinate system at each integration point in an element. The relationships between integration point and local co-ordinate system are illustrated in Figure 4.

7. NUMERICAL ANALYSIS I—UNIFORMLY DRIVEN SPHERICAL BEM MODEL

Two cases are tested with a uniformly driven spherical BEM model. The first case is for checking the validity of integration scheme on a curved surface and the other case is for comparing the calculated pressure distribution pattern with analytic solutions.

For the first case, pressure on the surface of a sphere which is uniformly driven is calculated (see Figure 5) and inspected if the resulting pressure is uniform on the surface. The sphere-shaped BEM model, whose radius is 5 m, has 1446 nodes and 2888, 3-node triangular elements (see Figure 5). As shown in Figure 6, the resultant pressure distribution is approximately uniform over the entire surface.

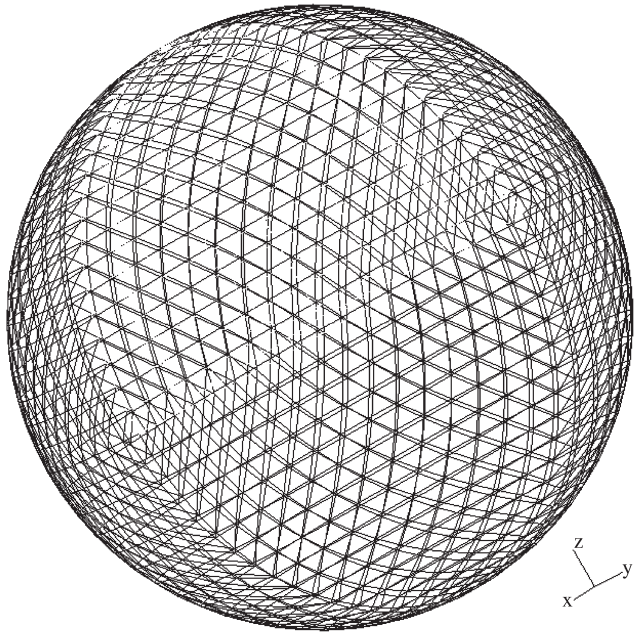

Figure 5. Uniformly driven spherical shape BEM model with 2,888 3-node triangular elements.

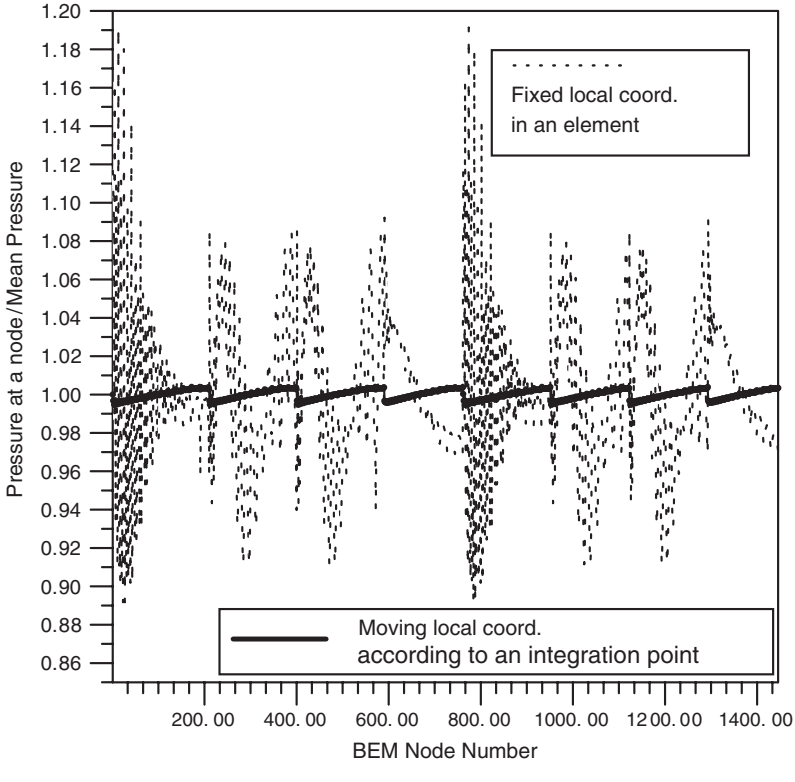

Figure 6. Pressure distributions on uniformly driven spherical surface.

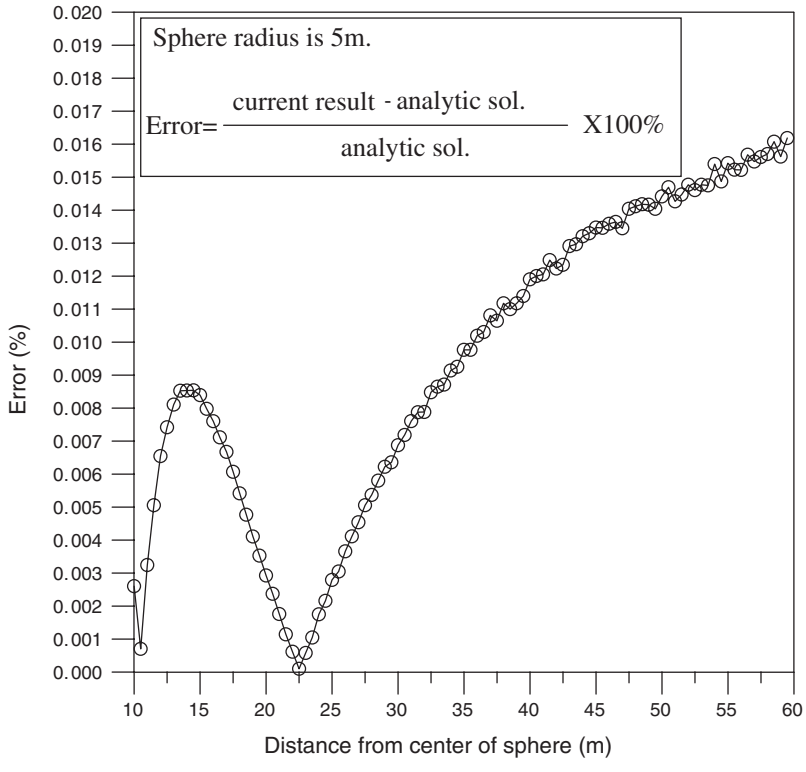

Figure 7. Comparison of current results with the analytic solution to see sound propagation of a uniformly driven sphere.

Now, for the second case, the pressure diffusion property of the spherical BEM model whose radius is 5 m is tested. We set frequencies, sound pressures and displacements on the surface to be the same as those of the fundamental solution of this model, and calculate the pressure distribution pattern with distance. As shown in equation (27) and (28), sound pressure and its first order derivative in the surface normal direction at $\mathbf{x}_s \sim (x_s, y_s, z_s)$ can be obtained from the analytic fundamental solution as follows.

$$p^*(\mathbf{x}, \mathbf{x}_s) = -\frac{\exp(-jk|\mathbf{x} - \mathbf{x}_s|)}{4\pi|\mathbf{x} - \mathbf{x}_s|}, \tag{27}$$

$$\frac{\partial p^*}{\partial n_s} = -(\mathbf{n}_s \cdot \mathbf{e}_R)\left[\frac{\exp}{4\pi R}\left[\frac{1}{R + \mathrm{j}k}\right]\right]. \tag{28}$$

A BEM model, consisted of 102 nodes and 200, 3-node triangular elements, is used to compute the error in pressure drop with distance. As shown in Figure 7, the computed values approximately correspond to the fundamental solutions.

8. NUMERICAL ANALYSIS II—RADIATION EFFICIENCY OF VIBRATING PLATE UNDER ONE-DIMENSIONAL FLOW

The radiation efficiency of a plate under one-dimensional flow is analytically calculated by Y. M. Chang and P. Leehey, and it is adopted in some papers for the verification of results [12].

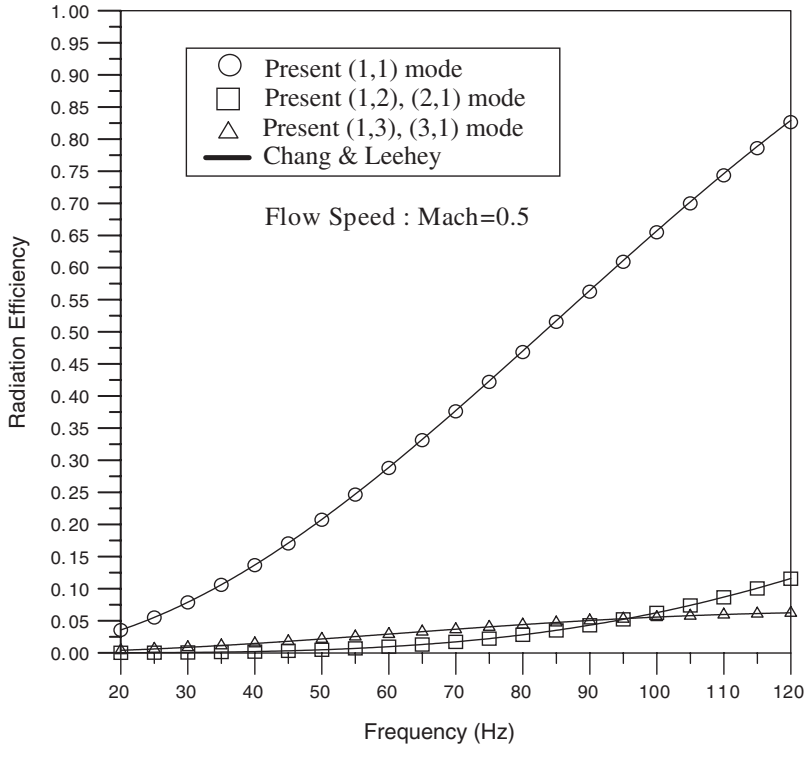

Figure 8. Radiation efficiency of simply supported plate at $M = 0{\cdot}5$.

The radiation efficiency, σ, is the ratio of acoustic powers of the current model and a baffled piston. [3] That is,

$$\sigma = \frac{\Pi}{\Pi_0} = \frac{\Pi}{\frac{1}{2}\rho_0 c A \langle v_n^2 \rangle}. \tag{29}$$

Sound power is defined as follows. [13]:

$$\Pi = \tfrac{1}{2}\int_S \mathrm{Re}[p^* v_n]\,\mathrm{d}S. \tag{30}$$

In this paper, an 1×1 m aluminum plate with elastic modulus $E = 70$ GPa, the Poisson ratio $\upsilon = 0{\cdot}3$ and density $\rho = 2700\,\mathrm{kg/m^3}$ is used. The fluid is assumed as air whose density is $1.21\,\mathrm{kg/m^3}$, and sound speed is 343 m/s. The results are presented in Figure 8. In Figure 8, the (m, n) mode means that the number of anti-nodes of mode shape in the longitudinal and the lateral direction are m and n respectively.

9. NUMERICAL ANALYSIS III—UNIFORMLY DRIVEN CYLINDRICAL SHELL

Three cylindrical BEM models are used to see variation patterns of radiated pressure according to the ratio of axial length and diameter. The diameters of three cylinders are 10 m and axial lengths are 20, 40 and 200 m, respectively, and the base and the top side are assumed to be covered with a rigid baffle. All of the BEM models have 32 nodes in the circumferential direction and 41 nodes along the axial direction.

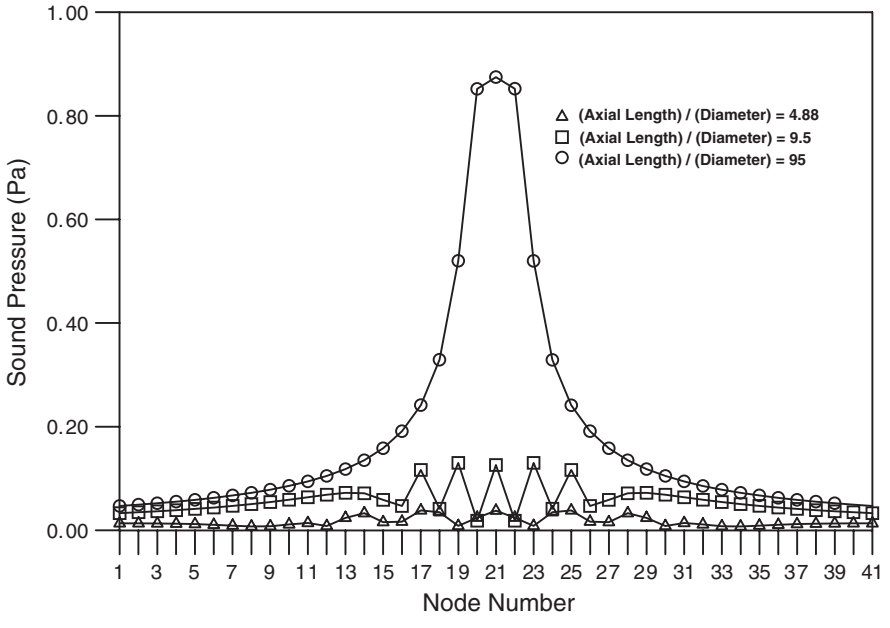

Figure 9. Several pressure distribution patterns depending on the ratio of cylinder's radius and axial length.

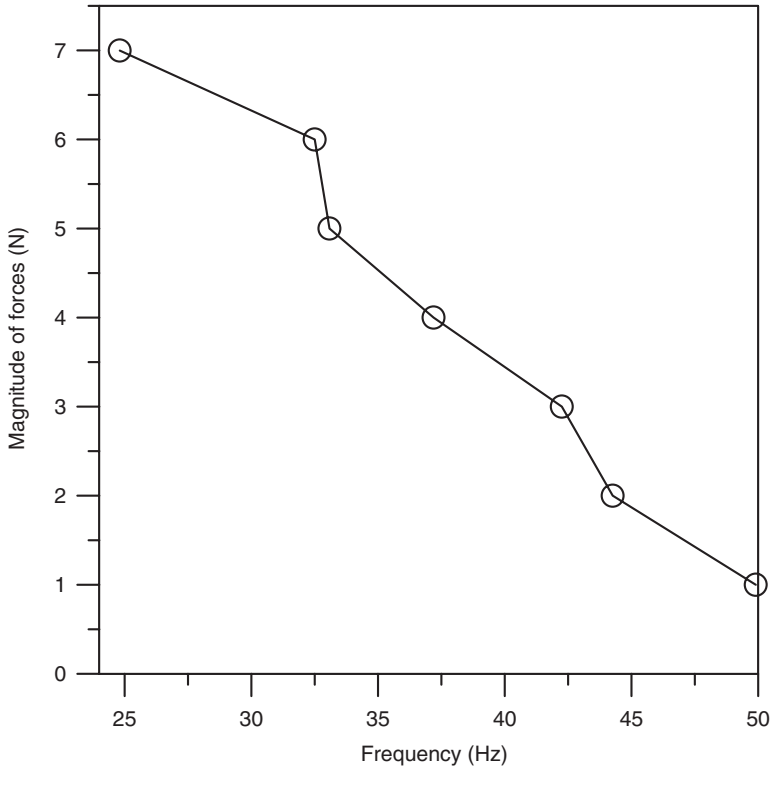

Figure 10. Magnitude of driven forces in the frequency domain.

It is found that there is no variation in the circumferential direction and pressures in the axial direction are distributed on surfaces of each cylinders as shown in Figure 9. In Figure 9, the distribution pattern becomes more independent of the end effect as the axial length is increased.

10. VIRTUAL EXPERIMENT—VIRTUAL INTERIOR SOUND FIELD OF A SIMPLY MODELLED AIRCRAFT CABIN

Usually, aircraft fuselage has been modelled simply as a cylindrical model [5, 14]. In this study, a cylindrical shell structure whose top and base sides are covered with a rigid baffle is adopted as a simple model of an aircraft fuselage. The radius of the model is 4·2 m, and its axial length is 20 m, and the thickness of fuselage skin is assumed as 1 mm. The FEM model has 448 nodes and 416 4-node square plate elements. The BEM models, which are composed of exterior and interior sound field models, have 416 nodes and 832 3-nodes triangular elements.

Appropriate frequencies at which sound pressure are calculated are selected by the concepts of structure-oriented analysis and human-oriented analysis. First, based on structure-oriented analysis, eigenvalues of the FEM model are obtained, and a frequency region that can be accepted to be reasonable with respect to the d.o.f. of FEM model is selected. Then by human-oriented analysis, some frequencies are selected in that frequency region. This time, the frequency domain is divided first by the ratio of the octave and then the domain between each musical interval is divided by the ratio of the octave again. Through these processes, 24·8, 32·5, 33·1, 37·2, 42·3, 44·3, and 50 Hz are selected.

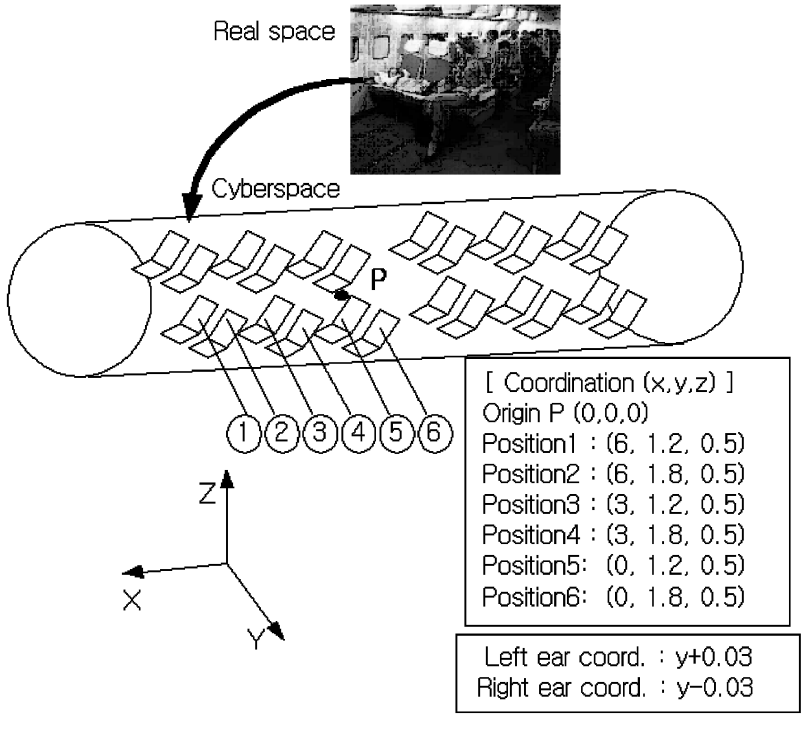

Figure 11. Definitions of positions in a virtual fuselage.

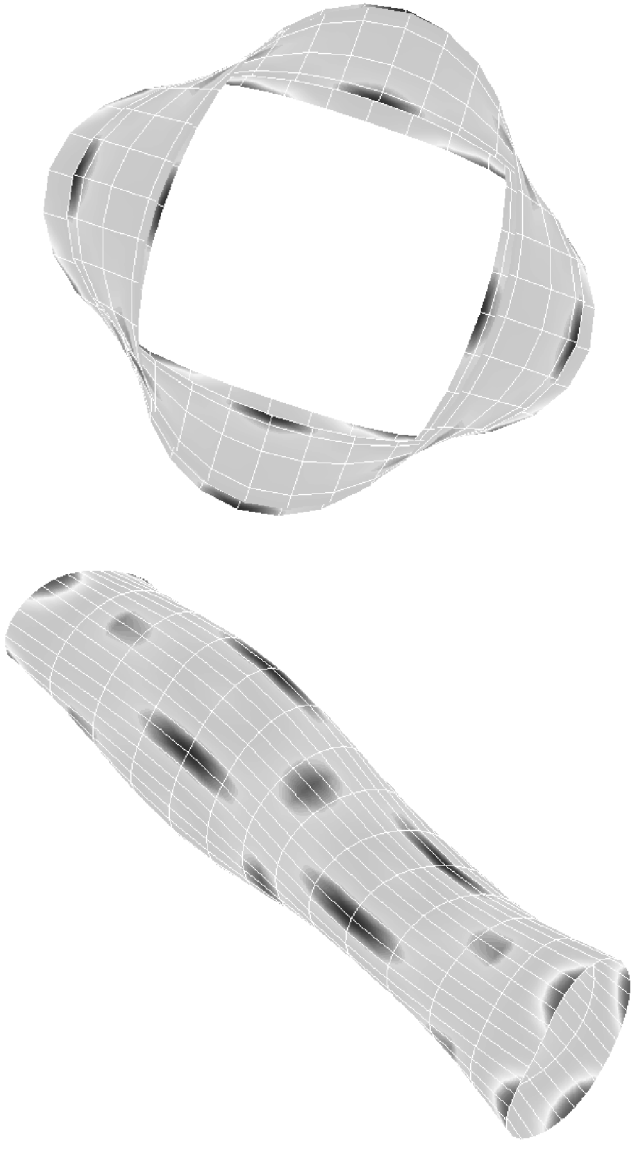

Figure 12. Mode shape of the cylinder at 50 Hz.

The fluid of the interior and exterior sound fields are assumed as air (its density is 1·21 kg/m^3 and speed of sound is 343 m/s) and the flow speed mach number of the exterior sound field is assumed as 0·4. The material of the cylinder is considered as Al2024-T3, so its elastic modulus E is 70 GPa, the Poisson ratio is 0·32075, and density is 2685 kg/m^3.

In this virtual experiment, the external forces are restricted to a low-frequency band because we consider forces generated from low-frequency flutter phenomenon of wings. Low-frequency forces given in Figure 10 are imposed on the cylinder at four points where the main wings are combined with the fuselage.

The sound pressures are calculated at six virtual seats. For stereo sound, sound at each ear is required for a seat. So sound pressures at 12 positions, as shown in Figure 11, are calculated. In Figure 12, the mode shape of the cylinder at 50 Hz is given. From the figure,

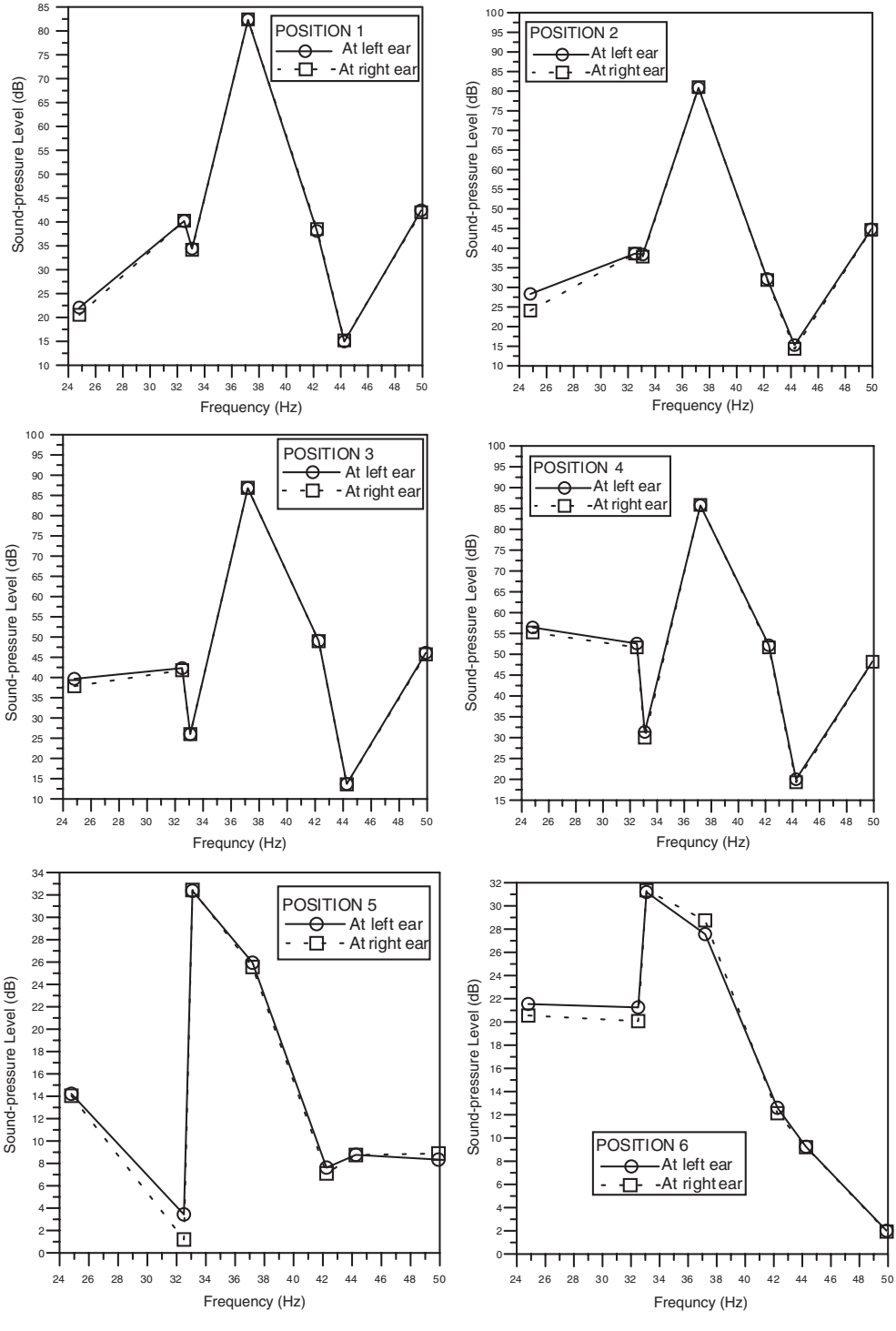

Figure 13. Sound-pressure level at each virtual seat.

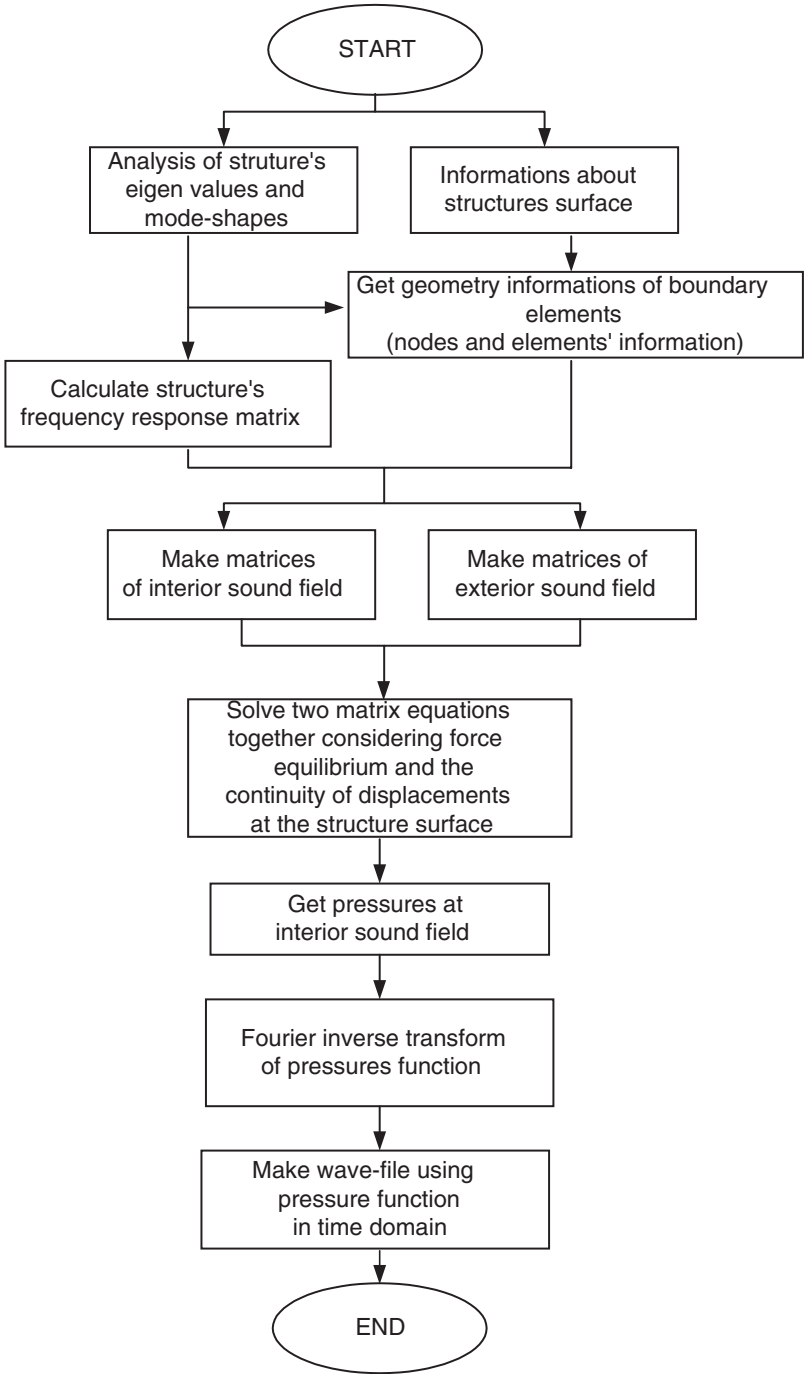

Figure 14. Algorithm of making virtual sound.

we can see that the region around the center of the cylinder in the axial direction is the node of vibration. So, the sound level is small at the center of the cylinder.

In Figure 13 sound pressure levels at each seat are given. When we hear the virtual sound, it feels not like sound but like a flow of wind because of its low frequency.

However, we can feel the characteristics of interior sound as if we are in a real aircraft. The process of this virtual experiment is summarized in Figure 14.

11. CONCLUDING REMARKS

In this study, virtual reality technology based on the exact physics is developed to produce sound in cyberspace. To realize the sound by computer simulation, two concepts, structure-oriented analysis and human-oriented analysis, are proposed. Boundary element method is used to calculate sound generated from vibrating structures. For integration on curved surfaces, an integration scheme is developed using global–local co-ordinates transformation. To confirm our developed scheme and check the applicability of the sound VR technology, several example problems are solved. For the verification of our scheme, sound pressure is calculated and compared with available analytic solutions and numerical results. In order to check the applicability of our scheme, a virtual experiment is performed: cabin noise realization of an aircraft is chosen as an application example.

Computation costs less than experiment. Also, extreme environments, which cannot be simulated in ordinary experimental environments, can be easily simulated in cyberspace. So, the proposed virtual reality technology of making sound has many benefits in the field of the design process concerning sound or noise.

ACKNOWLEDGMENTS

This study has been supported by the Ministry of Science & Technology through National Research Laboratory Programs.

REFERENCES

1. Y. M. Chang and P. Leehey 1979 *Journal of Sound and Vibration* **64**, 243–356. Acoustic impedance of rectangular panels.
2. C. E. Wallace 1972 *Journal of Acoustic Society of America* **51**, 946–952. Radiation resistance of a rectangular panel.
3. F. Fahy 1985 *Sound and Structural Vibration: Radiation, Transmission and Response*. New York: Academic Press, 101–109.
4. G. C. Everstine and F. M. Henderson 1980 *Journal of the Acoustical Society of America* **87**, 1938–1947. Coupled finite element/boundary element approach for fluid–structure interaction.
5. L. D. Pope, E.G. Wilby and J. F. Wilby 1987 *Journal of Sound and Vibration* **118**, 446-467. Propeller aircraft interior noise model, Part I: analysis model.
6. K. J. Bathe 1982 *Finite Element Procedures in Engineering Analysis*. Englewood Cliffs, NJ: Prentice-Hall Inc. .
7. S. F. Wu and L. Maestrello 1995 *American Institute of Aeronautics and Astronautics Journal* **33**, 13–19. Response of finite baffled plate to turbulent flow excitations.
8. W. S. Hall 1993 *The Boundary Element Method* Dordrecht: Kluwer Academic Publishers, pp. 161-175.
9. L. Meirovitch 1986 *Elements of Vibration Analysis*. New York: McGraw-Hill Inc., 2nd edition.
10. MacNeal-Schwendler Corporation, 1983 *MSC/NASTRAN Handbook For Dynamic Analysis*. MSC/NASTRAN Version 63.
11. Microsoft Company, *Microsoft Multimedia—New Multimedia Data Types and Data Techniques*, 15 April, 1994.
12. S. J. Kim and K. Y. Song 1999 *American Institute of Aeronautics and Astronautics Journal* **37**, 1180–1186. Active control of sound fields from plates in flow by piezoelectric sensor/actuator.

13. S. D. Snyder and N. Tanaka 1995 *Journal of Acoustical Society of America* **97**, 1702–1709. Calculating total acoustic power output using modal radiation efficiencies.
14. D.C. Mandic and J.D. Jones, 1991 *American Institute of Aeronautics and Astronautics Journal*, **29**, 1552–1561. Adaptive Active control of sound fields in elastic cylinders via vibrational inputs.

APPENDIX A: NOMENCLATURE

G	the Green function when one-dimensional flow exists
c	speed of sound
ψ	potential function
ω	angular velocity (rad/s)
k	wave number, ω/c
V	speed of flow
M	Mach number, V/c
p	sound pressure
u	displacement vector of structure
$\{U\}$	displacement vector of fluid
$\{v\}$	velocity vector of structure
$\{V\}$	velocity vector of fluid
x, y,z	components of a Cartesian co-ordinates in the $x-$, $y-$ and z-axis respectively
S	surface domain of a structure
$\{P\}$	sound pressure vector at the nodes on surface
Ω	sound field domain
α_{ij}	(i, j)th component of a structure's frequency response matrix
m_r	modal mass of the (r)th eigenvalues
$[T]$	square matrix which transfers d.o.f. of structure to d.o.f. of fluid and $[T][T]^{\mathrm{T}} = [E]$
$[B]$, $[C]$	square matrix
$[A_d]$	square matrix which transfers surface traction to equivalent concentrated load
$\omega(i)$	angular velocity of the (i)th selected mode
$p(i)$	calculated value of pressure in the (i)th selected mode
$[D]$	$-\mathrm{j}/\omega[C]$
$[Z]$	impedance matrix of structure
${}_m\phi_n$	(n)th element of (m)th eigenvector
Π	sound power
ρ_0	density of undisturbed fluid
$\langle V_n \rangle^2$	mean square of surface normal velocity
$\mathbf{x}$	position vector whose base is origin
$\dot{(\,)}$	time derivative of ( )
$(\,)_{fluid}$	value of fluid
$(\,)_s$	value on surface
$(\,)_R$	value in the radial direction
$(\,)_n$	(n)th element of vector ( )
$(\,)^*$	complex conjugate of complex number ( )
$(\,)_{pq}$	(p, q)th element of matrix ( )
$\hat{(\,)}$	value in frequency domain